Chemistry–A European Journal
Full Paper
doi.org/10.1002/chem.202005170
Chemistry Europe
European Chemical Societies Publishing

Electroceramics |Hot Paper|

Crystal Structure and Ferroelectric Evidence of $BaZnSi_3O_8$, a Low-Permittivity Microwave Dielectric Ceramic

Zheng-Yu Zou,[a] Xiao-Qiang Song,[a] Lei Jiang,[c] Chang-Lai Yuan,[d] Wen-Zhong Lu,[a, b] Yong-Ming Hu,[c] and Wen Lei*[a, b]

Abstract: $BaZnSi_3O_8$ ceramic was prepared by the conventional solid-state method and sintered at 1100 °C. XRD and synchrotron Rietveld refinement analyses revealed the $BaZnSi_3O_8$ ceramic presented a monoclinic structure with a space group of $P2_1/a$ (No.14), which is reported for the first time. The $BaZnSi_3O_8$ ceramic presented a weak ferroelectricity, which was confirmed by the *P–E* loop and the 90° nanoscale ferroelectric domain. Although ε_r–*T* displayed two ε_r abnormal peaks at 400 °C and 460 °C, the Curie temperature (T_c) was located at 460 °C according to the dielectric loss and Curie–Weiss law. Moreover, the $BaZnSi_3O_8$ ceramic exhibited optimized microwave dielectric properties with $\varepsilon_r = 6.55$, $Q \times f = 52400$ GHz, and $\tau_f = -24.5$ ppm/°C. Hence, the $BaZnSi_3O_8$ ceramic in the ternary BaO-ZnO-SiO_2 system possessed both weak ferroelectricity and microwave dielectric properties. These results are expected to break the technical barrier of ferroelectric phase shifter applications in microwave and even millimeter-wave frequency bands.

Introduction

Microwave dielectric ceramics are widely used as dielectric resonator (DR) antenna and filter devices owing to their excellent characteristics of low loss, high transmission rate, and size miniaturization.[1,2,3] In the extremely high-frequency millimeter-wave band, dielectric materials should possess low permittivity, very low dielectric loss, and near zero-temperature coefficients of resonant frequency, so as to improve the information transmission rate of devices, enhance the frequency selection, reduce the energy consumption, and ensure the working stability of resonant and transmission signals.[4,5] Ferroelectric ceramics are widely used in piezoelectricity,[6,7] electronic tunable devices,[8] energy storage,[9] and other fields because of their spontaneous polarization effect. However, the existence of domains in ferroelectric materials reduces the quality factor (*Q*) of microwave signal transmission, resulting in large dielectric loss. Therefore, the coexistence of ferroelectricity and microwave dielectric properties seems contradictory.

In recent years, many researchers have explored the potential applications of microwave-ferroelectricity tunable devices. Gu et al. selected a suitable substrate to exert weak tensile stress on $Ba_{0.8}Sr_{0.2}TiO_3$ ferroelectric films, resulting in large amounts of nanometer-scale domain structures with a low dielectric loss and realizing high electrical tunability of the material at microwave frequencies (1–8 GHz). This result breaks through the contradictory coexistence of ferroelectricity and microwave dielectric properties and is expected to be applied in electrically adjustable microwave phase shifters.[10] However, this complex structure needs to have weak tensile stress applied, which is a prerequisite that is difficult to achieve in practical applications. Lei et al. reported that $Ba_2Zn_{(1+x)}Si_2O_{(7+x)}$ ceramics possess both low-permittivity microwave dielectric properties and weak ferroelectricity.[11,12] According to dielectric theory, microdomain structures flip easily under an external electric field and their absorption of electromagnetic wave energy is low, thereby reducing dielectric loss.[13] Furthermore, the position, width, and strength of the Curie peak can be regulated by optimizing the lattice structure to obtain high electrical tunability characteristics. These ceramics are expected to break the barrier of the contradiction between the coexistence of ferroelectricity and microwave dielectric properties in dielectric materials. Moreover, a microwave ferroelectric phase shifter with a high stability, together with a highly integrated and independent phase control of each port can be prepared by using this kind of microwave-ferroelectric ceramic. Thus, microwave-ferroelectric ceramics may replace the traditional

[a] Z.-Y. Zou, X.-Q. Song, Prof. W.-Z. Lu, Prof. W. Lei
School of Optical and Electronic Information
Key Lab of Functional Materials for Electronic Information (B) of MOE
Huazhong University of Science and Technology
Wuhan 430074 (P. R. China)
E-mail: wenlei@hust.mail.edu.cn

[b] Prof. W.-Z. Lu, Prof. W. Lei
Wuhan National Laboratory for Optoelectronics
Huazhong University of Science and Technology
Wuhan 430074 (P. R. China)

[c] L. Jiang, Prof. Y.-M. Hu
Hubei Key Laboratory of Ferro-Piezoelectric Materials and Devices
Hubei University
Wuhan 430074 (P. R. China)

[d] Prof. C.-L. Yuan
Guangxi Key Laboratory of Information Materials
Guilin University of Electronic Technology
Guilin 541004 (P. R. China)

Supporting information and the ORCID identification number(s) for the author(s) of this article can be found under:
https://doi.org/10.1002/chem.202005170.

dielectric phase shifters applied in manufacturing base stations and radar antennas.

A previous study considered the $BaZnGeO_4$ ceramic with the same lattice structure as a typical weak ferroelectric material that undergoes six phase transitions during the cooling process, including the transition from the paraelectric phase to the ferroelectric phase near 827 °C.[14] Lattice structure parameters can be changed by ion substitution or by changing the stoichiometric ratio. Moreover, the temperature and intensity of the phase transition peak can be effectively adjusted to regulate ε_r against the temperature characteristics of the $BaZnSiO_4$ ceramic.[12] The Ba/Si ratio in the BaO-SiO_2 systems, such as $BaSiO_3$ (microwave dielectric properties: $\varepsilon_r = 11.1$, $Q \times f =$ 6643 GHz, $\tau_f = -35.4$ ppm/°C) and $Ba_5Si_8O_{21}$ (microwave dielectric properties: $\varepsilon_r = 7.26$, $Q \times f = 16\,694$ GHz, $\tau_f = +24.8$ ppm/°C), can also have an effective impact to adjust the position and intensity of the dielectric peaks.[15] The ε_r abnormal peaks of $BaSiO_3$ and $Ba_5Si_8O_{21}$ ceramics are located at 145 °C and −180 °C; hence, the position and intensity of ε_r abnormal peaks have a clear influence on the τ_f value. With regard to BaO-ZnO-SiO_2 systems, the Ba/Si ratio also affects the τ_f value. Song et al. reported that the $BaZnSi_3O_8$ ceramic has superior microwave dielectric properties ($\varepsilon_r = 6.55$, $Q \times f = 52\,401$ GHz, $\tau_f = -24.5$ ppm/°C) than $Ba_2ZnSi_2O_7$ ceramics.[16] Moreover, the $BaZnSi_3O_8$ ceramic shows signs of weak ferroelectricity similar to that of the $Ba_2ZnSi_2O_7$ ceramic. This observation warrants further investigation and confirmation. However, the $BaZnSi_3O_8$ phase was discovered by Segnit and Holland only in 1970.[17] They found that the $BaZnSi_3O_8$ ceramic has single but strong melting endotherm at 1130 °C. They also examined the XRD data of this type of ceramic. Kerstan et al. stated that $BaZnSi_3O_8$ phase crystallizing glass seals cannot be quantitatively analyzed in BaO-ZnO-SiO_2 systems because the crystal structure information of the $BaZnSi_3O_8$ phase has not been investigated yet.[18] Therefore, the crystal structural information of the $BaZnSi_3O_8$ ceramic is the key in studying the influence of lattice structure differences on the ε_r value against temperature characteristics.

This study comprehensively analyzes the phase constituents, crystal structural information, microstructure, and microwave dielectric properties of the $BaZnSi_3O_8$ ceramic. Furthermore, this study examined the evidence for ferroelectricity, such as *P–E* loop, Curie peak, and ferroelectric microdomains. The coexistence of weak ferroelectricity and low-permittivity microwave dielectric properties is emphasized to explore the evidence for the formation mechanism of weak ferroelectricity.

Results and Discussion

Owing to the lack of initial crystal structural information, a suitable crystal structure model was employed as the initial reference for $BaZnSi_3O_8$ XRD refinement.[19] The Rietveld refinement XRD patterns of $BaZnSi_3O_8$ ceramic sintered at 1100 °C are shown in Figure 1a. The refinement results revealed a single phase of the $BaZnSi_3O_8$ ceramic, which belongs to the monoclinic structure with a space group of $P2_1/a$ (No. 14). This phase was different from that of $CaZnSi_3O_8$ ceramics (triclinic, *P*

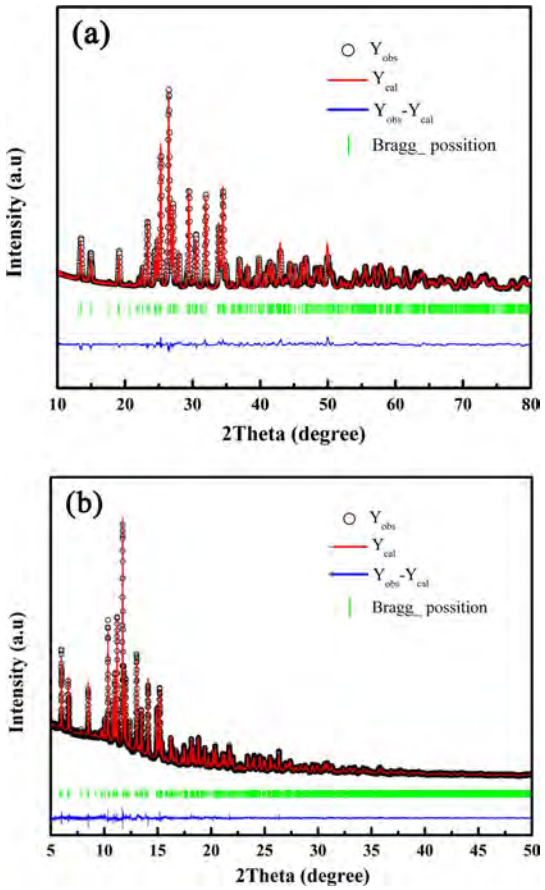

Figure 1. The Rietveld refinement of (a) XRD data and (b) synchrotron data of the $BaZnSi_3O_8$ ceramic sintered at 1100 °C.

[No. 2], $a = 8.121$ Å, $b = 12.927$ Å, $c = 7.206$ Å, $\alpha = 93.76°$, $\beta = 116.120°$, $\gamma = 84.368°$, $V = 675.7$ Å^3).[20] The observed and calculated values matched well, and the reliability of the refinement was proved by the Rietveld factors ($W_{Rp} = 11.3\%$, $Rp = 8.77\%$, $\chi^2 = 6.17$). The reliability of the crystal structural information of the $BaZnSi_3O_8$ ceramic was further verified by utilizing synchrotron XRD, which possesses high accuracy and intensity[21,22] at the wavelength of 0.6885 Å. The results are summarized in Figure 1b. The refinement of the synchrotron XRD data also proved the reliability of the crystal structure model. The lattice parameters extracted from the common XRD and synchrotron XRD patterns are listed in Table 1.

The lattice diagram of the $BaZnSi_3O_8$ ceramic sintered at 1100 °C for 3 h is depicted in Figure 2. The type of lattice structure belongs to barium feldspar, in which the [ZnO_4] tetrahedron is individually corner-connected with four [SiO_4] tetrahedrons, whereas three different connections are present in one [SiO_4] tetrahedron. The space of Zn^{2+} and Si^{4+} ions are relatively independent, in which 1/4 of the coordinated sites are tied up by Zn^{2+} and the remaining sites are tied up by Si^{4+}. The positions of non-tetrahedron are occupied by Ba^{2+} with a parallel arrangement of the (0 1 0) plane.[23] According to the atomic separation, the size of [ZnO_4] tetrahedrons is larger than that of [SiO_4] tetrahedrons, and the difference contributes to a slight distortion in [ZnO_4] tetrahedrons. The final atomic

Table 1. The lattice parameters of the monoclinic $BaZnSi_3O_8$ ceramic.[a]

	XRD	Synchrotron
a [Å]	8.725 ± 0.01	8.733 ± 0.005
b [Å]	13.072 ± 0.02	13.094 ± 0.01
c [Å]	7.307 ± 0.01	7.317 ± 0.01
α [°]	90.00	90.00
β [°]	115.85 ± 0.02	115.87 ± 0.02
γ [°]	90.00	90.00
V [Å^3]	752.9 ± 0.1	749.99 ± 0.05

[a] Space group: $P2_1/a$ (No. 14).

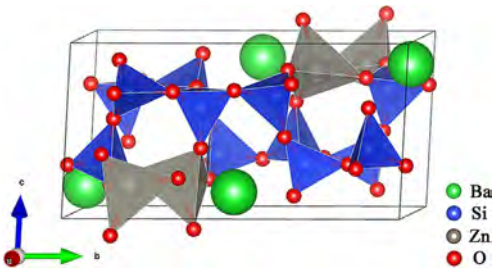

Figure 2. The crystal structure of the $BaZnSi_3O_8$ ceramic.

coordinates and bond length are presented in Tables 2 and 3. The average bond length of Zn–O (1.975 Å) and Si–O (1.617–1.622 Å) agreed well with that of melilite.[24]

The relationships among relative permittivity (ε_r), dielectric loss ($\tan\delta = 1/Q$), and temperature of the $BaZnSi_3O_8$ ceramic at different frequencies are illustrated in Figure 3a and b. Within the temperature range of 30 °C–325 °C, the relative permittivity linearly increased with temperature, whereas dielectric loss was maintained at a low order of magnitude. Electron and ionic displacement polarizations were the dominant factor within this temperature range. The first abnormal peak of permittivity occurred at 400 °C, whereas no abnormal performance was observed in the dielectric loss curves. At 460 °C, the second abnormal peaks in ε_r and $\tan\delta$ appeared in both low and high frequencies, indicating that these abnormal peaks were not caused by low-frequency space charges.[25] Hence,

Table 2. The final atomic coordinates of the $BaZnSi_3O_8$ ceramic.

Atom	Site	x	y	z	Occupancy	Biso.
Ba1	4e	0.275(12)	0.010(11)	0.135(15)	1.0	1.41
Zn1	4e	−0.125(3)	0.191(17)	0.187(3)	1.0	1.06
Si1	4e	0.976(7)	0.177(4)	0.736(8)	1.0	1.04
Si2	4e	0.185(7)	0.394(4)	0.305(7)	1.0	0.63
Si3	4e	0.783(8)	0.375(4)	0.619(8)	1.0	0.27
O1	4e	−0.013(14)	0.134(6)	−0.062(13)	1.0	0.32
O2	4e	0.126(8)	0.518(8)	0.278(10)	1.0	0.32
O3	4e	0.294(12)	0.376(7)	0.174(14)	1.0	0.32
O4	4e	0.648(12)	0.352(7)	0.724(13)	1.0	0.32
O5	4e	0.011(12)	0.340(7)	0.232(13)	1.0	0.32
O6	4e	0.944(11)	0.306(8)	0.719(12)	1.0	0.32
O7	4e	0.186(14)	0.122(6)	0.380(14)	1.0	0.32
O8	4e	0.805(14)	0.123(7)	0.554(16)	1.0	0.32

Table 3. The bond lengths of the $BaZnSi_3O_8$ ceramic.

Bond	Length [Å]	Av. length [Å]	Bond	Length [Å]	Av. Length [Å]
Ba1–O2	2.795(7)	2.758	Si2–O4	1.589(14)	1.621
Ba1–O5	2.694(10)		Si2–O6	1.700(12)	
Ba1–O1	2.847(11)		Si2–O1	1.537(12)	
Ba1–O3	2.791(10)		Si2–O8	1.656(11)	
Ba1–O7	2.680(12)		Si3–O8	1.674(11)	1.637
Ba1–O1	2.812(10)		Si3–O3	1.633(15)	
Zn1–O5	1.980(10)	1.934	Si3–O5	1.511(12)	
Zn1–O7	1.923(9)		Si3–O2	1.690(12)	
Zn1–O3	1.875(12)		Si4–O6	1.568(11)	
Zn1–O1	1.972(11)		Si4–O2	1.614(11)	1.613
			Si4–O4	1.691(15)	
			Si4–O7	1.578(11)	

the abnormal ε_r–T peaks at 460 °C may be attributed to the transition from the ferroelectric phase to the paraelectric phase.

The weak ferroelectricity of the $BaZnSi_3O_8$ ceramic was further verified by systematically testing the P–E loop as a necessary condition for ferroelectricity. According to the P–E loop checked at 1 kHz (Figure 3c), polarization monotonically increased as the electric field enlarged. However, Scott[26] attributed the formation of a 'banana-type' P–E loop to the influence of space charges and leakage currents that possess large loss and the Schottky effect between electrodes and pellets.[27] This effect was eliminated and intrinsic ferroelectric properties were further determined by polishing the samples and extracting 'positive-up-negative-down' measurements but excluding the influence of non-intrinsic factors.[28] As shown in Figure 3e, the remnant polarization was approximately 0.005 μC cm^{-2} with an electric field of 16 kV cm^{-1}. This result provided strong evidence for the weak ferroelectricity of the $BaZnSi_3O_8$ ceramic.[29] The polarization measurement above the phase transition temperature 460 °C is indeed helpful to verify the ferroelectricity, which requires further investigation.[30] TEM dark-field observation revealed a stripe-type domain (Figure 3f). The width of the domain structures ranged from 40 nm to 100 nm, which was similar to the weak ferroelectric properties of the $BaAl_2O_4$ and $Ba_2ZnSi_2O_7$ ceramics.[11,31,32]

The Curie–Weiss law describes the relationship between order parameter and symmetry at the Curie temperature (T_c).[33] According to the Curie–Weiss law, the permittivity between transition temperatures obeys the following equation [Eq. (1)]:

$$\varepsilon_r = C/(T - T_0) \quad (1)$$

where T_0 is the Curie–Weiss temperature; C is the modified Curie–Weiss constant, which represents the slope of the reciprocal of the permittivity versus temperature below T_c (C) and the temperature above T_c (C′); $C/C' > 4$ represents the first-order ferroelectric phase transition; and $C/C' < 4$ represents the second-order ferroelectric phase transition.[32] The Curie–Weiss fitting of $1/\varepsilon_r$ and the temperature below and above T_c for the $BaZnSi_3O_8$ ceramic at 2 MHz is shown in Figure 4. According to Figure 3a, the large dielectric loss from conduction significant-

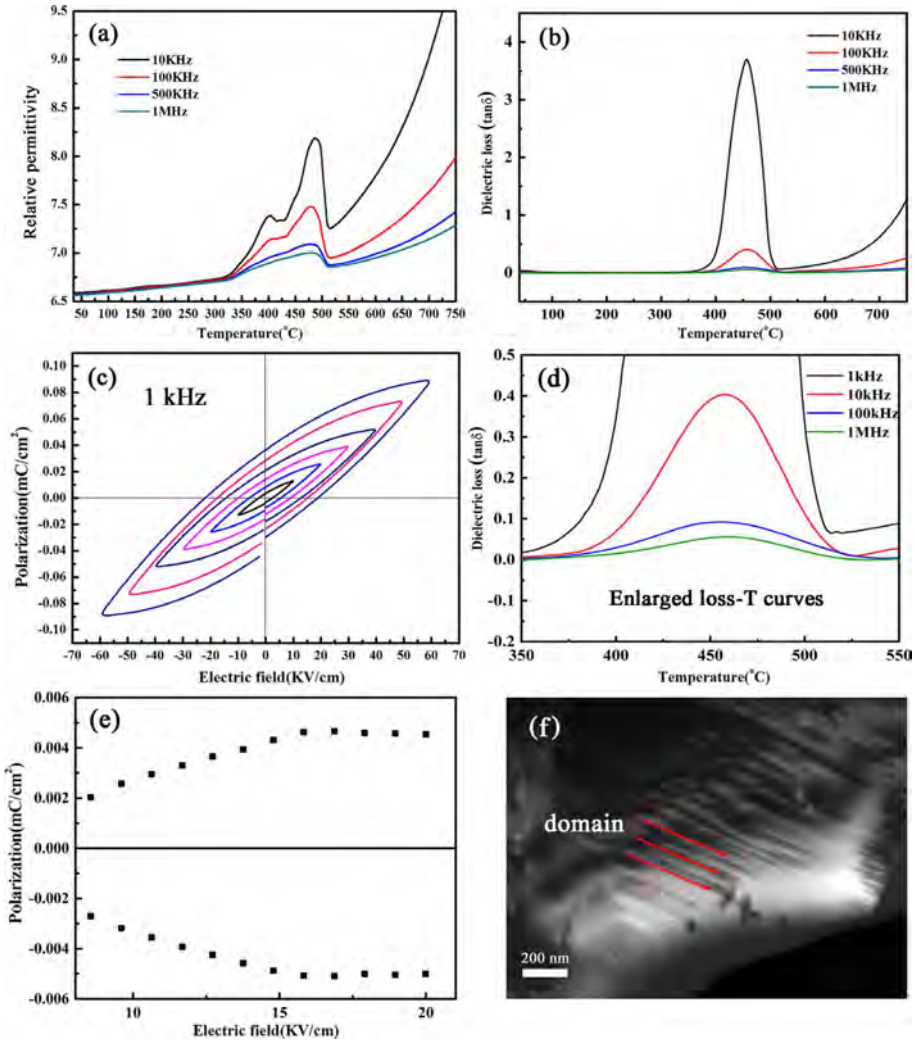

Figure 3. (a) Relative permittivity. (b,d) Dielectric loss as a function of temperature for the $BaZnSi_3O_8$ ceramic. (c) The *P*–*E* loop at 1 kHz. (e) The intrinsic remnant polarization of $BaZnSi_3O_8$ ceramic tested by PUND measurement. (f) The dark-field nano-scale domain structure.

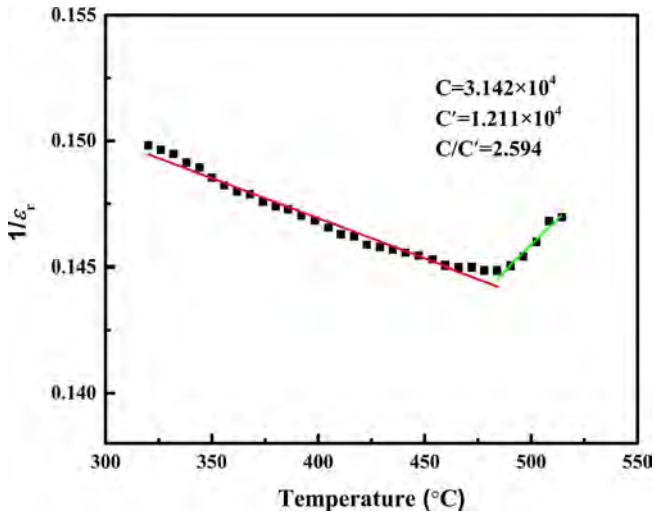

Figure 4. The Curie–Weiss fitting of $1/\varepsilon_r$ and temperature below and above T_c for the $BaZnSi_3O_8$ ceramic at 2 MHz.

ly increases the permittivity when the temperature is above 520 °C. To get accurate fitting results, 320–515 °C was selected as the temperature range. The fitting value of C/C′ was 2.594 for the $BaZnSi_3O_8$ ceramic, suggesting that the ceramic had a second-order ferroelectric phase transition at 460 °C.

The dark-field domain structures and selective-area electronic diffraction image recorded from the structure are presented in Figure 5. Given that a diffraction aperture selects different vectors (*g*), the dark-field domains at the axis zone of [001] presented noticeable changes in color contrast. For instance, the areas 'a_1', 'b_1', and 'c_1' were dark at the g_{200} vector, but the color contrast became the opposite as the vector transformed to g_{020}, illustrating that a 90° domain could be obtained at the axis zone of [001].

Further evidence of the weak ferroelectricity of the $BaZnSi_3O_8$ ceramic was obtained by piezoresponse force microcopy (PFM).[34] The stripe-type domains could be distinctly seen in the topography graph (Figure 6 a). The amplitude signal (Fig-

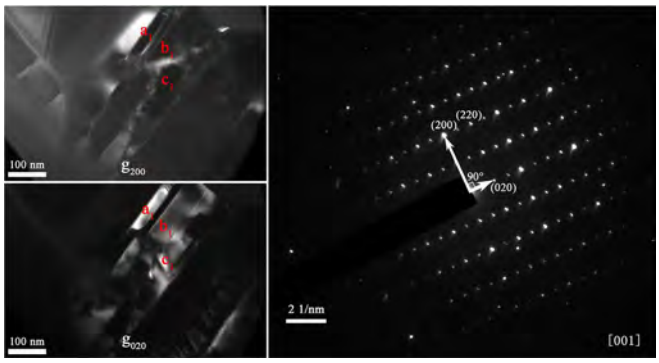

Figure 5. The dark-field domain structures and selective-area electronic diffraction image of the $BaZnSi_3O_8$ ceramic.

ure 6b) represents the amplitude of the piezoelectric response, and the color contrast of amplitude signal was determined by the grain's crystallography orientation.[35] The shade in the phase signal (Figure 6c) reflects the direction of polarization.[36] In Figure 6c, the bright region in the phase image represents a 'positive' polarization vector, the direction of which was perpendicular upwards to the surface. By contrast, the dark region reflects a 'negative' polarization vector, the direction of which was perpendicular downwards into the bulk. Notably, the changing directions of color contrast in the amplitudes and phase signals were consistent with the arrangement direction of the domains in topography image. PFM analysis confirmed that the stripe-type domain with a width of 150–200 nm actually existed in the $BaZnSi_3O_8$ ceramic. In addition, the ampli-

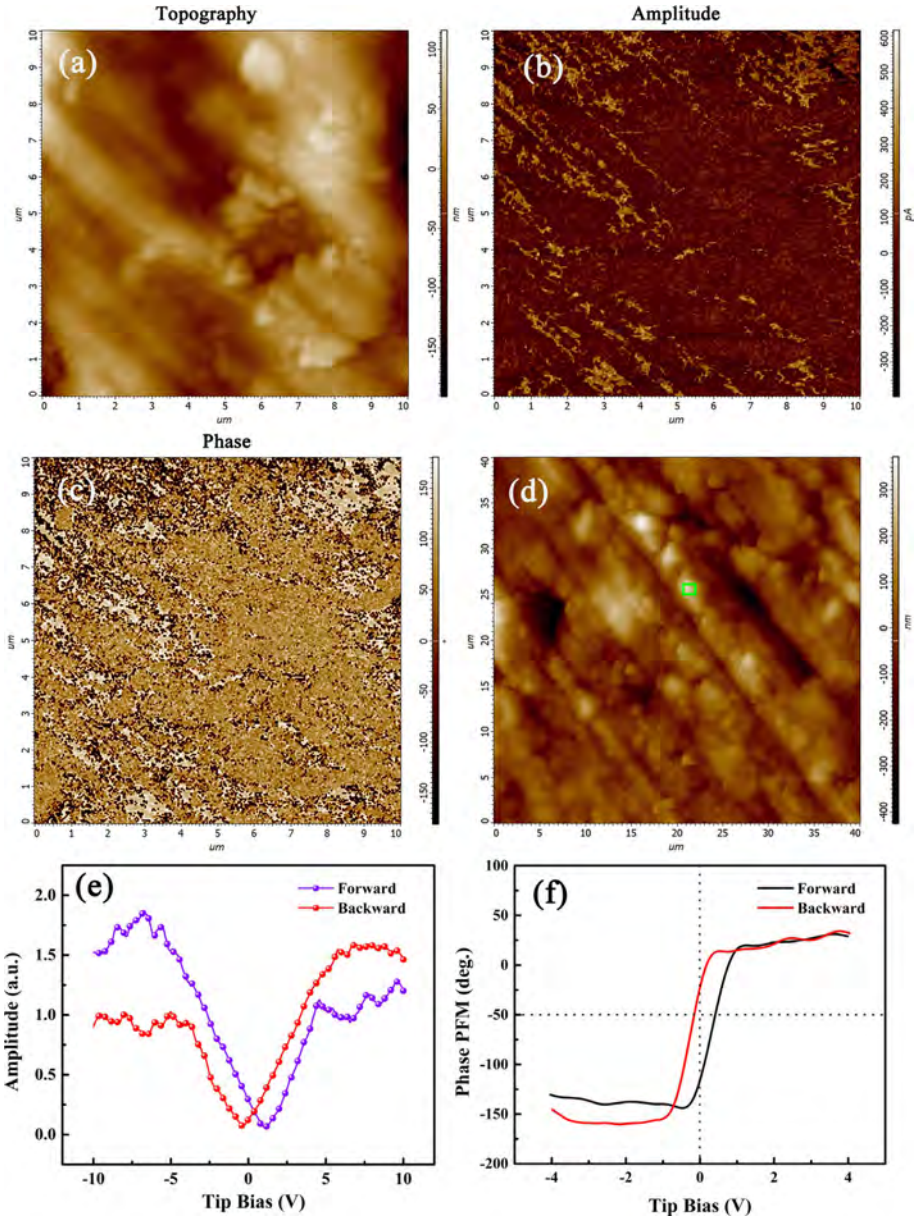

Figure 6. (a,d) Topography, (b) amplitude, and (c) phase PFM images of the $BaZnSi_3O_8$ ceramic. The (e) amplitude and (f) phase versus voltage curves of the $BaZnSi_3O_8$ ceramic.

tude versus voltage curves (Figure 6e) showed a butterfly-type loop, and the phase of the selected region (Figure 6f) also indicated a clear hysteresis phenomenon. These results confirmed the existence of ferroelectricity in the $BaZnSi_3O_8$ ceramic.[37] Taniguchi et al.[38] discovered that twisting of the $[SiO_4]$ tetrahedron and the distortion of the Bi_2O_2 sublattice may result in soft mode displacements in Bi_2SiO_5 ceramics, a condition that may further induce spontaneous polarization inside the structure. By comparison, the twisting of silicate tetrahedral chains had a certain universality in silicates, such as $BaZnSiO_4$, $Ba_2ZnSi_2O_7$, and $BaSiO_3$.[11,12] $BaCoSiO_4$ and $BaCo_{0.75}Si_{0.75}Fe_{0.5}O_4$ were also proved to be ferroelectric ceramics owing to the twisting of B and C tetrahedral sites. This characteristic has little contribution to the macroscopic polarity and therefor presents weak ferroelectricity.[39] Moreover, the mechanism of spontaneous polarization is different from that of conventional ferroelectric materials and the spontaneous polarization mechanism of the $BaZnSi_3O_8$ ceramic warrants further investigation.

Excellent microwave dielectric properties ($\varepsilon_r = 6.55$, $Q\times f = 52\,400$ GHz, $\tau_f = -24.5$ ppm/°C) were achieved in the $BaZnSi_3O_8$ ceramic sintered at 1100 °C for 3 h. To further check the relationship between microstructure and microwave dielectric properties, the SEM images and the microwave dielectric properties of $BaZnSi_3O_8$ ceramics sintered at different temperatures are shown in Figure S1 and Table S1, respectively (in the Supporting Information). A dense microstructure with grain sizes of 1–2 μm and the optimum microwave dielectric properties were obtained at 1100 °C. The generation of the liquid phase significantly reduced the $Q\times f$ value with the temperature above 1100 °C. The results are consistent with the performance parameters reported by Song et al.[16] The microwave dielectric properties comparison of $BaZnSi_3O_8$ and reported silicates is given in Table 4. Compared with the $Ba_2ZnSi_2O_7$ ceramic, the $BaZnSi_3O_8$ ceramic possesses better microwave dielectric properties and lower sintering temperatures. Therefore, the $BaZnSi_3O_8$ ceramic has broader potential applications in microwave ferroelectric devices and regulation of ε_r (or resonant frequency) stability against temperature.

Table 4. The typical sintered temperature (ST) and microwave dielectric properties of silicate ceramics.

Compositions	ST [°C]	ε_r	$Q\times f$ [GHz]	τ_f [ppm/°C]
$Zn_{1.8}SiO_{3.8}$[40]	1300	6.60	147000	−22.0
$(Mg_{0.4}Zn_{0.6})_2SiO_4$[41]	1400	6.60	95600	−60.0
$Ba_2ZnSi_2O_7$[11]	1200	8.09	26600	−51.4
$HfSiO_4$[42]	1600	7.00	25000	−44.0
Al_2SiO_5[43]	1525	4.43	41800	−17.0
$Ca_3MgSi_2O_8$[44]	1350	13.10	27000	−62.0
$BaZnSi_3O_8$	1100	6.55	52400	−24.5

Conclusion

In this study, a single-phase $BaZnSi_3O_8$ microwave-ferroelectric ceramic was prepared by the conventional solid-state method at 1100 °C. Rietveld refinement analysis revealed that the as-prepared ceramic possesses a monoclinic structure with a space group of $P2_1/a$ (No. 14). The coexistence of weak ferroelectricity and microwave dielectric properties were also found in the $BaZnSi_3O_8$ ceramic. The Curie temperature (T_c) was located at 460 °C, and the intrinsic remnant polarization was approximately 0.005 μC cm^{-2}. Nanoscale ferroelectric domains with a 90° direction were also observed by TEM and PFM. The $BaZnSi_3O_8$ ceramic also exhibited optimized microwave dielectric properties with $\varepsilon_r = 6.55$, $Q\times f = 52\,400$ GHz, $\tau_f = -24.5$ ppm/°C. Therefore, the $BaZnSi_3O_8$ microwave ferroelectric ceramic has great potential for tunable applications in microwave frequency bands.

Experimental Section

The $BaZnSi_3O_8$ ceramic was prepared by the conventional solid-state method by using reagent-grade $BaCO_3$ (99.8%), ZnO (99.5%), and SiO_2 (99.5%) powders as raw materials. According to the desired stoichiometry, the raw materials were weighed and ground in a ball mill in a polyethylene jar for 5 h by using ZrO_2 balls with deionized water. After drying at 85 °C, the mixtures were calcined in air at 1000 °C for 3 h at a heating rate of 5 °C min^{-1}. The powders were then uniaxially pressed into samples 12 mm in diameter and approximately 6 mm in height under 150 MPa. The samples were sintered at the densification temperature of 1090–1120 °C for 3 h at a heating rate of 5 °C min^{-1} in air. Subsequently, the samples were cooled at a rate of 2 °C min^{-1} down to 1000 °C and then naturally cooled in a furnace.

XRD and synchrotron data were obtained by X-ray diffraction (XRD, XRD-7000, Shimadzu, Kyoto, Japan) by using $Cu_{K\alpha}$ radiation, whereas synchrotron diffraction data were collected with the beamline BL11U. Crystal structural information was extracted by Rietveld refinement[45] by using the FullProf software. The ε_r–T graph was plotted by using an Agilent 4294A impedance analyzer (Agilent, Santa Clara, USA) and a VDMS-2000 measuring system (Partulab, Wuhan, China). The P–E loop was identified by using a radiant multiferroic device (RT66B, Shimadzu, Radiant Technologies, USA). The positive-up-negative-down (PUND) test was performed to eliminate the influence of leakage on the FE loop. In the PUND method, five rectangle voltage pulses are applied to the specimens. The first pulse is negative, and it pre-polarizes the specimen to a known negative state. The second to fifth pulses are denoted as 'positive', 'up', 'negative', and 'down', respectively. The 'positive' and 'negative' pulses contain the FE and non-FE contributions, whereas the 'up' and 'down' currents contain only the non-FE contributions. Subtraction of two polarization responses yields the intrinsic remanent polarization, which indicates the dependable FE contributions.[46,47] Ferroelectric domains were observed by transmission electron microscopy (TEM, Tecnai G2 F30, FEI, the Netherlands) and piezoresponse force microscopy (PFM, NT-MDT, Russia). ε_r and unloaded $Q\times f$ values were measured at about 12.5 GHz in the TE_{011} mode by the Hakki and Coleman method[48] by using a network analyzer (Agilent E8362B, Agilent Technologies, Santa Clara, USA) and parallel silver boards. The τ_f value within the temperature range of 25 °C to 80 °C was calculated by Equation (2):

$$\tau_f = \frac{1}{f(T_0)}\frac{[f(T_1) - f(T_0)]}{T_1 - T_0} \quad (2)$$

where $f(T_1)$ and $f(T_0)$ represent the resonant frequencies at T_1 (80 °C) and T_0 (25 °C), respectively.

Acknowledgments

This work was supported by the National Natural Science Foundation of China (NSFC-52072133, 51772107), the Equipment Development Department of China (1807WM0004), the Major Programs of Technical Innovation in Hubei Province of China (2018AAA039), and the Innovation Team Program of Hubei Province, China (2019CFA004). The authors are grateful to the Analytical and Testing Center, Huazhong University of Science and Technology, for TEM analysis. The authors are also grateful to Prof. Xiaojun Kuang and Prof. Zhenxiang Cheng for crystallographic structural analysis and synchrotron Rietveld refinement analysis.

Conflict of interest

The authors declare no conflict of interest.

Keywords: crystal structure · electroceramics · ferroelectricity · silicate

[1] D. Zhou, D. Guo, W. B. Li, L. X. Pang, X. Yao, D. W. Wang, I. M. Reaney, *J. Mater. Chem. C* **2016**, *4*, 5357 – 5362.
[2] D. Zhou, L. X. Pang, D. W. Wang, C. Li, B. B. Jin, I. M. Reaney, *J. Mater. Chem. C* **2017**, *5*, 10094 – 10098.
[3] H. F. Zhou, X. H. Tan, J. Huang, N. Wang, G. C. Fan, X. L. Chen, *J. Alloy. Compd.* **2017**, *696*, 1255 – 1259.
[4] H. W. Chen, H. Su, H. W. Zhang, T. C. Zhou, B. W. Zhang, J. F. Zhang, X. L. Tang, *Ceram. Int.* **2014**, *40*, 14655 – 14659.
[5] J. X. Bi, C. C. Li, Y. H. Zhang, C. F. Xing, C. H. Yang, H. T. Wu, *Mater. Lett.* **2017**, *196*, 128 – 131.
[6] Z. M. Fan, X. L. Tan, *J. Eur. Ceram. Soc.* **2018**, *38*, 3472 – 3477.
[7] K. Yang, C. S. Yang, X. X. Yang, Y. H. Tan, Y. Z. Tang, W. J. Lei, *Chem. Eur. J.* **2020**, *26*, 5887 – 5892.
[8] M. W. Cole, P. C. Joshi, M. H. Ervin, *J. Appl. Phys.* **2001**, *89*, 6336 – 6340.
[9] J. Fu, Y. D. Hou, X. P. Liu, M. P. Zheng, M. K. Zhu, *J. Mater. Chem. C* **2020**, *8*, 8704 – 8731.
[10] Z. Q. Gu, S. Pandya, A. Samanta, S. Liu, G. Xiao, C. J. G. Meyers, A. R. Damodaran, H. Barak, A. Dasgupta, S. Saremi, A. Polemi, L. Y. Wu, A. A. Podpirka, A. Will-Cole, C. J. Hawley, P. K. Davies, R. A. York, I. Grinberg, L. W. Martin, J. E. Spanier, *Nature* **2018**, *560*, 622 – 627.
[11] Z. Y. Zou, X. K. Lan, W. Z. Lu, G. F. Fan, X. H. Wang, X. C. Wang, P. Fu, W. Lei, *Ceram. Int.* **2016**, *42*, 16387 – 16391.
[12] Z. Y. Zou, Z. H. Chen, X. K. Lan, W. Z. Lu, B. Ullah, X. H. Wang, W. Lei, *J. Eur. Ceram. Soc.* **2017**, *37*, 3065 – 3071.
[13] X. Lv, X. X. Zhang, J. G. Wu, *J. Mater. Chem. A* **2020**, *8*, 10026 – 10073.
[14] T. Nagai, S. Asai, R. Okazaki, I. Terasaki, H. Taniguchi, *Solid State Commun.* **2015**, *219*, 12 – 15.
[15] W. Lei, Z. Y. Zou, Z. H. Chen, B. Ullah, Z. Aurang, X. K. Lan, W. Z. Lu, G. F. Fan, X. H. Wang, X. C. Wang, *J. Am. Ceram. Soc.* **2018**, *101*, 25 – 30.
[16] X. Q. Song, W. Z. Lu, X. C. Wang, X. H. Wang, G. F. Fan, R. Muhammad, W. Lei, *J. Eur. Ceram. Soc.* **2018**, *38*, 1529 – 1534.
[17] E. R. Segnit, A. E. Holland, *Aust. J. Chem.* **1970**, *23*, 1077 – 1085.
[18] M. Kerstan, C. Thieme, A. Kobeisy, C. Rüssel, *J. Mater. Sci.* **2017**, *52*, 1789 – 1796.
[19] C. L. Diao, C. H. Wang, N. N. Luo, Z. M. Qi, T. Shao, Y. Y. Wang, J. Lu, Q. C. Wang, X. J. Kuang, L. Fang, F. Shi, X. P. Jing, *J. Appl. Phys.* **2014**, *115*, 114103.
[20] M. Heuer, K. Bente, M. Steins, A. Rothkopf, *Z. Kristallogr. NCS* **1998**, *213*, 691 – 692.
[21] A. J. Rodriguez, S. Chaturvedi, J. C. Hanson, A. Albornoz, J. L. Brito, *J. Phys. Chem. B* **1998**, *102*, 1347 – 1355.
[22] L. J. Zhang, P. Qin, C. Han, J. L. Wang, Z. H. Ge, Q. Sun, Z. X. Cheng, Z. Li, S. X. Dou, *J. Mater. Chem. A* **2018**, *6*, 2507 – 2516.
[23] M. Kerstan, M. Müller, C. Rüssel, *J. Solid State Chem.* **2012**, *188*, 84 – 91.
[24] T. Tamura, A. Yoshiasa, K. Iishi, S. Takeno, H. Maeda, S. Emura, K. Koto, *Phys. Chem. Minerals* **1996**, *23*, 81 – 88.
[25] Z. J. Song, K. X. Song, L. Bing, P. Zheng, H. B. Bafrooei, W. Su, H. X. Lin, F. Shi, D. W. Wang, I. M. Reaney, *Appl. Ceram. Tech.* **2020**, *17*, 771 – 777.
[26] L. Pintilie, M. Alexe, *Appl. Phys. Lett.* **2005**, *87*, 112903.
[27] J. F. Scott, *J. Phys. Condens. Matter* **2008**, *20*, 021001.
[28] V. R. Reddy, S. K. Upadhyay, A. Gupta, A. M. Awasthi, S. Hussain, *Ceram. Int.* **2014**, *40*, 8333 – 8339.
[29] F. Liu, J. Li, Q. Li, Y. Wang, X. Zhao, Y. Hua, C. Wang, X. Liu, *Dalton Trans.* **2014**, *43*, 1691 – 1698.
[30] T. Kimura, Y. Sekio, H. Nakamura, T. Siegrist, A. P. Ramirez, *Nat. Mater.* **2008**, *7*, 291 – 294.
[31] H. T. Stokes, C. Sadate, D. M. Hatch, L. L. Boyer, M. J. Mehl, *Phys. Rev. B* **2002**, *65*, 064105.
[32] J. Li, X. K. Lan, X. Q. Song, W. Z. Lu, X. H. Wang, F. Shi, W. Lei, *Dalton Trans.* **2019**, *48*, 3625 – 3634.
[33] S. Kaur, A. K. Thakur, A. Choudhary, A. M. Biradar, *Appl. Phys. Lett.* **2005**, *87*, 102507.
[34] R. F. Zhu, Q. H. Zhang, B. J. Fang, S. Zhang, X. Y. Zhao, J. N. Ding, *Appl. Phys. Lett.* **2018**, *112*, 122902.
[35] D. Gobeljic, V. V. Shvartsman, A. Belianinov, B. Okatan, S. Jesse, S. V. Kalinin, C. Groh, J. Rödel, D. C. Lupascu, *Nanoscale* **2016**, *8*, 2168 – 2176.
[36] H. Y. He, X. Lu, M. C. Li, Y. M. Wang, Z. R. Li, Z. G. Lu, L. Lu, *J. Mater. Chem. C* **2020**, *8*, 2411 – 2418.
[37] X. D. Yan, M. P. Zheng, X. Gao, M. K. Zhu, Y. D. Hou, *J. Mater. Chem. C* **2020**, *8*, 13530 – 13556.
[38] H. Taniguchi, A. Kuwabara, J. Kim, Y. Kim, H. Moriwake, S. Kim, T. Hoshiyama, T. Koyama, S. Mori, M. Takata, H. Hosono, Y. Inaguma, M. Itoh, *Angew. Chem. Int. Ed.* **2013**, *52*, 8088 – 8092; *Angew. Chem.* **2013**, *125*, 8246 – 8250.
[39] A. Bhim, J. P. Sutter, J. Gopalakrishnan, S. Natarajan, *Chem. Eur. J.* **2020**, *27*, 1995 – 2008.
[40] N. H. Nguyen, J. B. Lim, S. Nahm, J. H. Paik, J. H. Kim, *J. Am. Ceram. Soc.* **2007**, *90*, 3127 – 3130.
[41] K. X. Song, X. M. Chen, C. W. Zheng, *Ceram. Int.* **2008**, *34*, 917 – 920.
[42] J. Varghese, T. Joseph, K. P. Surendran, T. P. D. Rajan, M. T. Sebastian, *Dalton Trans.* **2015**, *44*, 5146 – 5152.
[43] I. J. Induja, M. T. Sebastian, *J. Eur. Ceram. Soc.* **2017**, *37*, 2143 – 2147.
[44] H. B. Bafrooei, B. Liu, W. T. Su, K. X. Song, *Mater. Lett.* **2020**, *263*, 127248.
[45] H. M. Rietveld, *J. Appl. Crystallogr.* **1969**, *2*, 65 – 71.
[46] J. Liu, X. Q. Liu, X. M. Chen, *J. Appl. Phys.* **2016**, *119*, 204102.
[47] S. Horiuchi, R. Kumai, Y. Tokura, *Adv. Mater.* **2011**, *23*, 2098 – 2103.
[48] B. W. Hakki, P. D. Coleman, *IRE Trans. Microw. Theory Technol.* **1960**, *8*, 402 – 410.

Manuscript received: December 2, 2020
Revised manuscript received: January 14, 2021
Accepted manuscript online: January 18, 2021
Version of record online: March 4, 2021